Society of Medical Education & Research

2021, Volume 1, Issue 1, Page No: 171-188

ISSN: 3108-4834

Archive of International Journal of Cancer and Allied Science

Macrophage CCL7 Drives Colorectal Cancer Immunotherapy Resistance by Modulating Macrophage and CD8⁺ T Cell Infiltration

Marco Antonio Bianchi[1]*, Luca Francesco Romano[1], Giulia Elena Conti[1]

[1]Department of Experimental Oncology, University of Milan, Milan, Italy.

***E-mail** ✉ m.bianchi.oncology@outlook.com

Abstract

Although immune checkpoint inhibitors (ICIs) have emerged as a transformative approach in cancer immunotherapy, their clinical benefit in colorectal cancer (CRC) remains modest. Elucidating the mechanisms that underlie resistance to ICIs in CRC is critical for identifying novel therapeutic targets. To dissect the role of CCL7 in CRC, we employed myeloid-specific Ccl7 knockout mice alongside MC38 tumor-bearing models. Tumor tissues were analyzed using proteomics, RNA sequencing, and flow cytometry to examine the impact of CCL7 on the immune landscape within the tumor microenvironment.

Our findings reveal that CRC tumors with high infiltration of CCL7-expressing tumor-associated macrophages (TAMs) exhibit reduced responsiveness to ICIs. Loss of CCL7 in myeloid cells diminished immunosuppressive TAM populations and facilitated the recruitment of activated CD8+ T cells into the tumor. Mechanistic studies demonstrated that CCL7 drives peroxisome formation and fatty acid oxidation in TAMs, reinforcing their immunosuppressive behavior through the PI3K-AKT-PEX3 pathway. Additionally, CCL7 suppresses the AKT2-STAT1-CXCL10 signaling axis, limiting CD8+ T cell infiltration. Therapeutically, CCL7 inhibition delayed tumor growth and synergized with anti-PD-L1 therapy to enhance antitumor effects. This study identifies CCL7+ TAMs as key mediators of ICI resistance in CRC and delineates the molecular circuits involved, supporting CCL7 as a promising combinatorial target to improve immunotherapy outcomes.

Keywords: Immunotherapy, Immune checkpoint inhibitor, Colorectal cancer, Tumor microenvironment (TME), Macrophage

Introduction

Colorectal cancer (CRC) ranks among the most common cancers worldwide, standing fourth in incidence and third in cancer-related mortality [1]. While immune checkpoint inhibitors (ICIs), particularly those targeting PD-1/PD-L1, have shown promising clinical benefits in CRC patients with high microsatellite instability or defective mismatch repair (MSI-H/dMMR), a substantial proportion—up to 50%—of metastatic MSI-H/dMMR patients fail to respond, often leading to disease progression and relapse [2].

Access this article online https://smerpub.com/

Received: 03 August 2021; **Accepted:** 21 November 2021

How to cite this article: Bianchi MA, Romano LF, Conti GE. Macrophage CCL7 Drives Colorectal Cancer Immunotherapy Resistance by Modulating Macrophage and CD8⁺ T Cell Infiltration. Arch Int J Cancer Allied Sci. 2021;1:171-88. https://doi.org/10.51847/cK3obzkwMW

The tumor immune microenvironment (TIME) has emerged as a key determinant of immunotherapy success in CRC [3]. Its suppressive characteristics allow tumor cells to evade immune surveillance, thereby facilitating tumor initiation, progression, metastasis, recurrence, and resistance to treatment [4]. Understanding the cellular and molecular composition of this immunosuppressive microenvironment is essential for developing novel strategies aimed at reversing immune evasion and improving therapeutic outcomes [5]. The TIME comprises a dynamic network of tumor cells, immune cells, secreted factors, extracellular matrix elements, and metabolic molecules [3]. Notably, immunosuppressive myeloid populations, including tumor-associated macrophages (TAMs) and myeloid-derived suppressor cells (MDSCs), are abundant within CRC tumors and have been shown to promote tumor growth, metastasis, and therapy resistance [6, 7]. TAMs, in particular, contribute to tumor progression by expressing immune checkpoint molecules and releasing cytokines,

chemokines, and growth factors that support malignant behavior [8].

C-C motif ligand 7 (CCL7), also known as monocyte chemoattractant protein-3, is a chemokine originally identified in human osteosarcoma cell supernatants [9]. Elevated CCL7 expression recruits monocytes to sites of inflammation, enhancing local immune responses and exacerbating inflammatory disease symptoms [10]. Importantly, CCL7 is overexpressed in multiple cancers, including CRC and non-small cell lung cancer, and is associated with aggressive tumor traits such as proliferation, epithelial-mesenchymal transition, invasion, and metastatic spread [11, 12]. Studies indicate that high CCL7 levels in CRC cells promote invasive and metastatic phenotypes [13, 14]. Mechanistically, CCL7 interacts with receptors such as CCR1, CCR2, and CCR3, triggering downstream signaling via JAK-STAT and ERK-JNK pathways to enhance CRC cell proliferation, migration, and invasion [15, 16]. While much of the research has focused on CCL7's role in tumor cell growth and motility, recent evidence suggests that MDSC-derived CCL7 also plays a significant role in CRC progression [17]. Despite these insights, the functions of CCL7 within the TIME of CRC remain poorly defined.

The present study investigates the contribution of tumor-infiltrating myeloid cells to immunotherapy resistance in CRC. We demonstrate that higher levels of CCL7-expressing TAMs are associated with poor responses to anti-PD-1/PD-L1 treatment. These CCL7+ macrophages modulate both the recruitment and activation of tumor-infiltrating macrophages and CD8+ T cells, ultimately influencing ICI effectiveness. Additionally, we evaluated the therapeutic potential of targeting CCL7 to suppress CRC growth and enhance the efficacy of immune checkpoint blockade.

Materials and Methods

Acquisition of human samples and data

Tumor and adjacent normal colorectal tissues were collected at Chongqing University Cancer Hospital (Chongqing, China). Peripheral blood was also obtained from CRC patients and healthy volunteers. All sample collection and experimental procedures were performed under ethical approval from Chongqing University Cancer Hospital (Ethics Number CZLS2023114-A), and written informed consent was obtained from all participants or their guardians, following the Declaration of Helsinki. RNA sequencing datasets comprising 594 CRC cases were retrieved from the PanCancer Atlas via cBioPortal, while single-cell RNA sequencing datasets were accessed through GEO. After filtering out samples missing AJCC stage or survival data, 440 pre-treatment cases were retained for further analysis.

Cell culture and experimental reagents

THP1, LLC, CT26, and MC38 cell lines were obtained from the Type Culture Collection of the Chinese Academy of Sciences (Shanghai, China) in 2020, and HT29 cells were sourced from Wuhan Pricella Biotechnology (Wuhan, China; CL-0118). Cell morphology and functional integrity were routinely verified, and all lines were confirmed mycoplasma-free. Luciferase-expressing MC38 and CT26 cell lines (MC38-luc, CT26-luc) were generated in our laboratory. Bone marrow-derived macrophages (BMDMs) were prepared as described previously [8]. All cells were cultured in high-glucose DMEM supplemented with 10% FBS and 100 U/mL penicillin/streptomycin. Recombinant mouse CCL7 was obtained from PeproTech (Cat No. 250–08), and BEZ235 was sourced from Selleck (Cat No. S1009).

Animal models and tumor experiments

Ccl7-floxed (Ccl7f/f) mice and Lyz2cre mice on a C57BL/6 background were obtained from Shanghai Biomodel Organism Center. Myeloid-specific Ccl7 knockout (Ccl7 MKO) mice were generated by crossing Ccl7f/f with Lyz2cre mice and genotyped according to the supplier's instructions. Age-matched male and female C57BL/6 and BALB/c mice (6–8 weeks old) were purchased from the Animal Institute of the Academy of Medical Sciences (Beijing, China). Mice were housed under pathogen-free conditions on a 12-hour light/dark cycle with standard chow. For tumor establishment, 5×10^5 MC38-luc or CT26-luc cells were injected intraperitoneally into Ccl7f/f, Ccl7 MKO, or wild-type mice. Tumor progression was monitored every 3–4 days using an IVIS Lumina imaging system, normalizing photon emission to baseline measurements. TAM depletion was performed via intraperitoneal injection of 200 µL clodronate liposomes (Apexbio, Cat No. K2721) one day before tumor inoculation and every 3 days thereafter. Oral gavage of Bindarit (5 mg/kg, Cat No. HY-B0498, MCE) was administered every 3 days once tumors were detectable. For therapeutic studies, recombinant CCL7 (50 µg/kg, Cat No. 250–08,

PeproTech), anti-Ccl7 antibody (100 µg, Cat No. AF-456-NA, R&D Systems), or anti-PD-L1 antibody (200 µg, Cat No. BE0101, BioXcell) was administered intraperitoneally three days post-tumor injection. All procedures complied with national and international regulations and were approved by the IACUC of Chongqing University Cancer Hospital (Ethics Number SYXK2021-001).

Flow cytometry analysis

Tumor tissues were dissociated into single-cell suspensions and incubated on ice for 20 minutes in PBS containing 2% FBS. Cells were stained with fluorophore-conjugated antibodies (1:100) for 30 minutes on ice. Dead cells were excluded using Fixable Viability Dye Efluor 780 (Cat No. 65-0865-14; eBioscience). Surface markers included CD45, CD8α, IFN-γ, granzyme B, CD3, CD4, CD11b, Gr-1, CD11c, MHC II, F4/80, B220, PD-L1, NK1.1, CCR1, CCR2, and CCR3 (all from Biolegend, San Diego, CA). For intracellular markers ARG1 (Cat No. 42284, GeneTex) and iNOS (Cat No. MA5-17139, Thermo), cells were fixed and permeabilized using the Foxp3/Transcription Factor Staining Kit (Cat No. 00-5523-00, eBioscience) prior to intracellular staining. CD8+ T cell proliferation and functional assays were performed as previously described [8]. Cells were harvested, washed twice with PBS, resuspended in 500 µL PBS, and labeled with CFSE (Dojindo, Cat No. C309). Data were acquired on a BD FACS Canto II and analyzed using FlowJo v10.

Lipidomic profiling

BMDMs (2×10^6) from Ccl7f/f, Ccl7 MKO, and wild-type mice were cultured with or without CCL7 for 24 hours. Adherent cells were collected for lipidomic analysis according to previously established protocols [8].

Seahorse metabolic analysis

BMDMs (2×10^4) were plated in Seahorse XFe96 Spheroid Microplates, and their oxygen consumption rate (OCR) was quantified using an Agilent Seahorse XFe96 Analyzer according to the manufacturer's instructions.

Migration assays

Conditioned medium was collected from Ccl7f/f and Ccl7 MKO TAMs cultured in RPMI 1640 with 2.5% FBS for 48 hours. Subsequently, 5×10^4 CD8+ T cells isolated from C57BL/6 mouse spleens were seeded in the upper chamber of Matrigel-coated (0.4 mg/mL; BD Biosciences) 24-well Transwell plates (Corning, Cat No. 07-200-149), with TAM-conditioned medium in the lower chamber serving as a chemoattractant. After 24 hours, migrated T cells were fixed and quantified under a microscope. For in vivo migration, 1×10^6 CD8+ T cells labeled with CFSE (Dojindo, Cat No. C309) were intravenously injected into Ccl7f/f and Ccl7 MKO mice 15 days post-MC38 tumor implantation. Eighteen hours later, tumors were harvested, processed into single-cell suspensions, and analyzed by flow cytometry following surface staining.

Transfection experiments

Control siRNAs (siNC) and siRNAs targeting mouse Pex3, Ccr1, Ccr2, and Ccr3 were purchased from RiboBio (Guangzhou, China). Pex3 overexpression lentiviruses were acquired from GeneChem (Shanghai, China). Transfections were performed using Lipofectamine RNAiMAX (Thermofisher, Cat No. 13778150) following the manufacturer's protocol. Knockdown or overexpression efficiency was confirmed via qPCR or Western blot.

ELISA

Serum or conditioned media levels of Ccl7, Ccl6, Ccl17, Ccl12, and Cxcl10 were measured using mouse or human ELISA kits (Solarbio Life Science) according to the manufacturer's instructions.

Quantitative real-time PCR (qPCR)

Total RNA was extracted using RNAiso Plus (Cat No. 9108Q, Takara) and quantified. One microgram of RNA was reverse-transcribed into cDNA using the PrimeScript RT-PCR Kit (Cat No. RR014A, Takara). qPCR was performed with TB Green Fast qPCR Mix (Cat No. RR430A, Takara), with all reactions run in triplicate. Primer sequences were obtained from PrimerBank (https://pga.mgh.harvard.edu/primerbank/).

Immunofluorescence

Human and mouse CRC tissues were fixed in 4% formaldehyde for 15 minutes, blocked with 10% normal goat serum for 1 hour, and incubated overnight at 4°C with primary antibodies against CD68 (1:100; Cat No. ab53444, Abcam), CCL7 (1:50; Cat No. MA5-29089, Invitrogen), and PMP70 (1:100; Cat No. sab4200181, Sigma-Aldrich). Secondary antibodies Anti-rat IgG Alexa Fluor 488 (Cat No. 4416, CST) and Anti-rabbit

IgG Alexa Fluor 647 (Cat No. 4414, CST) were applied at 1:200 for 1 hour. Nuclei were counterstained with DAPI (100 ng/mL), and images were captured using a Leica TCS SP5 confocal microscope.

RNA-seq library preparation

TAMs from MC38 tumor-bearing Ccl7f/f and Ccl7 MKO mice were used to isolate total RNA. Strand-specific RNA-seq libraries were prepared, with mRNA enriched through two rounds of poly(A+) selection using Dynabeads oligo-(dT)25 (Invitrogen), followed by sequencing on an Illumina NovaSeq 6000 platform.

Proteomic analysis

TAMs (5×10^6) from MC38 tumor-bearing Ccl7f/f and Ccl7 MKO mice were collected and sent to Novogene Co., Ltd. (Beijing, China) for proteomic profiling.

Western blotting

Cells were lysed in RIPA buffer and incubated on ice for 30 minutes. Lysates were centrifuged at 13,000×g for 15 minutes at 4°C, and supernatants were collected. Western blot analysis was performed as described previously [8]. Primary antibodies included CCL7 (1:1,000; Cat No. PA5-86885, Invitrogen), Pex3 (1:1,000; Cat No. 30424-1-AP, Proteintech), Acox1 (1:1,000; Cat No. 10957-1-AP, Proteintech), p-PI3K (1:1,000; Cat No. 4228, CST), PI3K (1:1,000; Cat No. 4249T, CST), p-AKT1 (1:1,000; Cat No. 2938, CST), AKT1 (1:1,000; Cat No. 9018, CST), AKT2 (1:1,000; Cat No. 3063, CST), Stat1 (1:1,000; Cat No. 9172, CST), and β-actin (1:1,000; Cat No. A1978, Sigma-Aldrich).

Statistical analysis

Details of statistical methods and sample sizes are provided in figure legends. All experiments were independently repeated at least three times, with data reported as mean ± SD. Comparisons between two groups were performed using the Mann-Whitney test, while one- or two-way ANOVA with Sidak's multiple comparisons test was used for multiple groups (GraphPad Prism v8.0). Kaplan-Meier analysis and log-rank testing were applied for survival analyses. A p-value <0.05 was considered statistically significant.

Results and Discussion

Increased CCL7+ macrophages in CRC correlate with poor ICIs response and reduced patient survival

We postulated that tumor-infiltrating myeloid cells might contribute to immunotherapy resistance in CRC. To test this, we analyzed a previously published scRNA-seq dataset of immune cells from CRC patients who were either responsive or non-responsive to neoadjuvant ICIs treatment [18]. Examination of the tumor-infiltrating myeloid compartments revealed notable differences in cell subset composition between responders and non-responders **(Figures 1a and 1b)**. To investigate the contribution of these populations to ICIs resistance, we assessed differentially expressed genes across myeloid cells in the two patient groups. Tumor-infiltrating myeloid cells from non-responders exhibited elevated expression of several chemokines, including CXCL1, CXCL3, CXCL5, CCL7, and CCL20, compared with responders **(Figure 1c)**. Given the marked upregulation of CCL7 in non-responsive tumors, we focused on the CCL7+ myeloid subset.

Analysis indicated that CCL7 transcripts were highly enriched in tumor-infiltrating myeloid cells and upregulated in CRC tissues, with expression observed across multiple cell types, including macrophages, dendritic cells, and fibroblasts [19]. Among these, a distinct macrophage subset exhibited predominant CCL7 expression. Further scRNA-seq analyses of an independent CRC cohort confirmed that CCL7+ macrophages were significantly expanded in ICI-resistant samples. Quantification revealed that the number of CCL7+ macrophages was higher in tumor tissues than in adjacent non-tumor tissues **(Figure 1d)**. Notably, their accumulation increased with CRC progression, and elevated infiltration of CCL7+ macrophages was associated with poorer overall survival **(Figures 1e and 1f)**.

In addition, CRC patients displayed higher serum CCL7 levels compared with healthy controls **(Figure 1g)**, and an increased fraction of CCL7+ macrophages was detected in peripheral blood **(Figure 1h)**. Immunofluorescence further confirmed enrichment of CCL7 within CD68+ macrophages in tumor tissues **(Figure 1i)**. Similarly, MC38 tumor tissues showed a greater proportion of CCL7+ macrophages relative to the spleen **(Figure 1j)**, and serum CCL7 levels positively correlated with MC38 tumor size **(Figure 1k)**. Collectively, these findings demonstrate that CCL7+ TAMs are enriched in CRC and their presence is associated with diminished responsiveness to ICIs therapy.

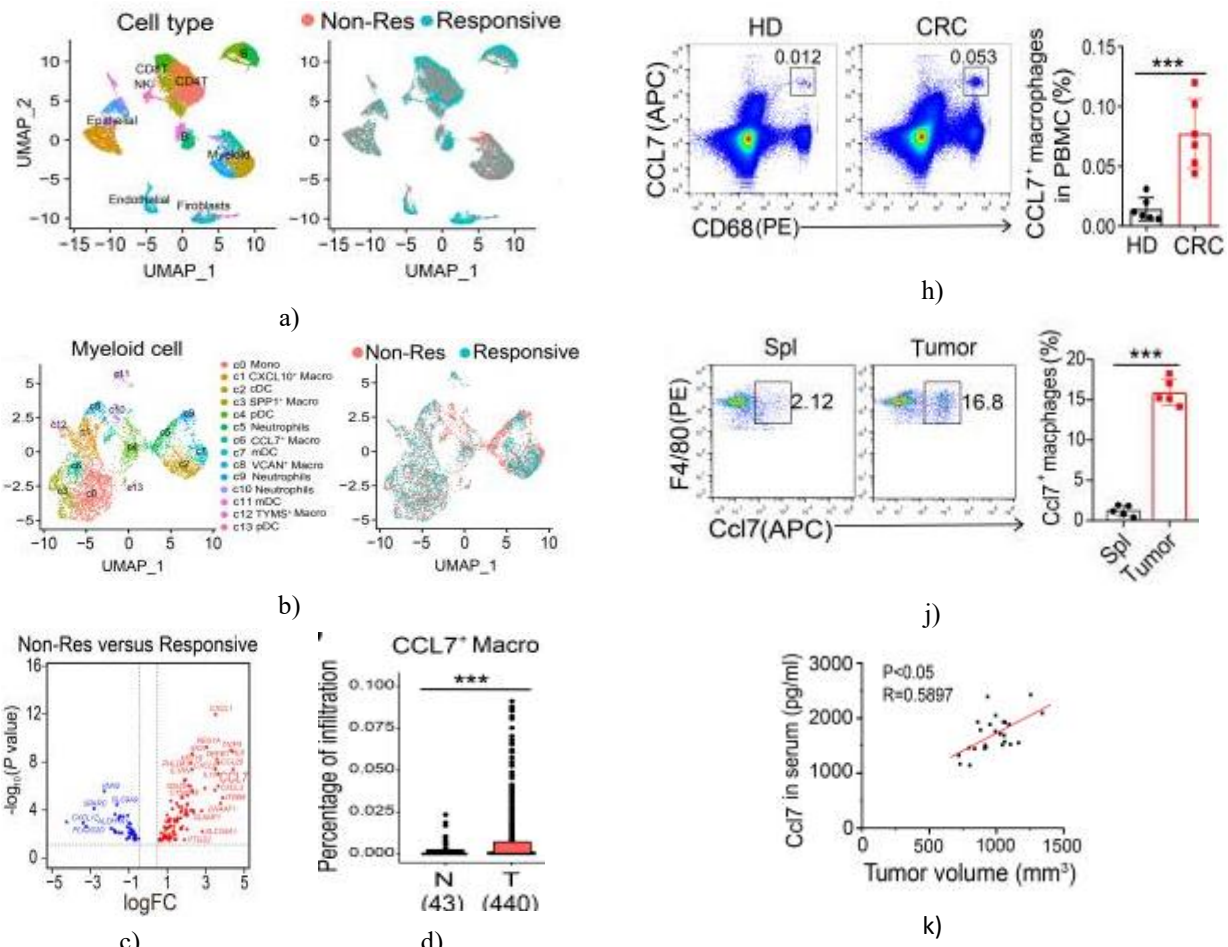

Figure 1. Abundance of CCL7+ TAMs in CRC tissues is associated with ICI resistance in patients. (a) Broad cell populations in CRC patients who were either non-responsive or responsive to ICIs were identified through unsupervised clustering using the GSE205506 dataset. (b) Subpopulations of myeloid cells within the clusters shown in (a). (c) Differentially expressed genes among myeloid cells comparing non-responsive and responsive CRC samples. (d) Quantification of CCL7+ TAMs in tumor tissues and adjacent non-tumor CRC tissues. (e) Analysis of CCL7+ TAM frequencies across CRC stages. (f) Survival probabilities of CRC patients stratified by the expression of the CCL7+ TAM signature normalized to CD68. (g) ELISA measurement of serum CCL7 in healthy donors (HD) and CRC patients (n=5). (h) Flow cytometry showing CCL7+ TAMs in peripheral blood from CRC patients versus HD (n=6). (i) Immunofluorescence of CCL7 in CD68+ macrophages in tumor (T) and adjacent normal tissues (N); red = CCL7, green = CD68, blue

= DAPI. Scale bar, 5 μm. (j) Flow cytometric analysis of CCL7+ macrophage proportions in spleen (Spl) and MC38 tumors (n=5). (k) Correlation between serum CCL7 levels and MC38 tumor volume (n=25) assessed using Pearson's correlation. Data are mean ± SD. Significance: *p<0.05, **p<0.01, ***p<0.001 (Mann-Whitney test). Abbreviations: CRC, colorectal cancer; FCM, flow cytometry; ICI, immune checkpoint inhibitor; TAMs, tumor-associated macrophages.

CCL7 modulates the accumulation and function of tumor-infiltrating macrophages in CRC progression

Given the association between CCL7+ macrophages and ICIs resistance, as well as their accumulation during CRC progression, we next explored their contribution to tumor growth. Myeloid-specific Ccl7 knockout mice (Ccl7 MKO) were generated. Compared with Ccl7f/f controls, Ccl7 MKO mice developed smaller tumors in both intraperitoneal and subcutaneous MC38 models **(Figure 2a)**. Additionally, LLC tumors in Ccl7 MKO mice grew more slowly , suggesting that macrophage-derived Ccl7 promotes tumor progression. Correspondingly, serum Ccl7 concentrations were markedly lower in Ccl7 MKO tumor-bearing mice than in Ccl7f/f controls **(Figure 2b)**. To examine how Ccl7 influences the tumor immune microenvironment, we analyzed immune cell infiltration in tumors by flow cytometry. Ccl7 MKO tumors displayed significantly increased CD8+ T cell infiltration **(Figure 2c)**, and the proportion of IFN-γ+ CD8+ T cells was also elevated **(Figure 2d)**. In contrast, tumor-infiltrating dendritic cells, MDSCs, and macrophages were reduced in Ccl7 MKO tumors **(Figures 2e–2i)**. Notably, the percentage of M1-like iNOS+ macrophages increased, whereas M2-like Arg1+ macrophages decreased in the absence of Ccl7 **(Figures 2j and 2k)**. Further characterization of TAMs in MC38 tumors revealed that CCL7+ TAMs expressed higher levels of M2 markers, such as CD206 and Arg1, and lower levels of M1-associated markers, including ROS, MHC II, iNOS, and CD86

Consistent with these observations in mice, CRC patients with higher tumor CCL7 expression exhibited increased M2-like macrophage infiltration and reduced CD8+ T cell presence **(Figure 2l)**. Collectively, these results indicate that TAM-derived CCL7 plays a pivotal role in modulating both the accumulation and activity of tumor-infiltrating macrophages and CD8+ T cells, thereby impacting tumor progression.

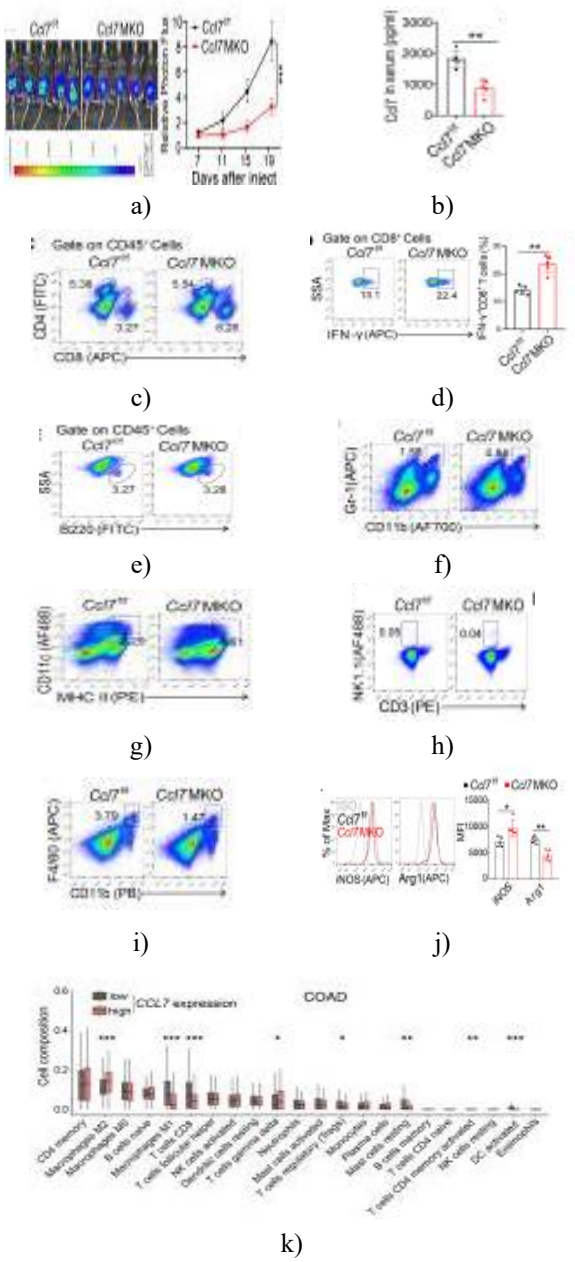

Figure 2. CCL7 influences tumor-infiltrating CD8+ T cells and macrophage dynamics. (a, b) MC38-luc cells (5×10^5) were administered intraperitoneally into Ccl7f/f and Ccl7 MKO mice, with tumor growth monitored every four days (a). Corresponding serum levels of Ccl7 were determined via ELISA (b, n=5). (C–I) Fourteen days post-tumor inoculation, mice were sacrificed and tumor-infiltrating immune populations were quantified by flow cytometry, including total T cells (c), IFN-γ+ CD8+ T cells (d), B cells (e), MDSCs (f), dendritic cells (g), NK cells (h), and macrophages (i) (n=5 per group). (j) iNOS and Arg1 expression in macrophages was measured

to assess M1 versus M2 polarization (n=5). (k) Comparative statistical analysis of immune cell subsets between Ccl7f/f and Ccl7 MKO tumors. (l) In colon adenocarcinoma (COAD) patient samples, tumors with high CCL7 expression displayed distinct immune infiltration patterns relative to low-expression tumors. Data are presented as mean ± SD; significance: *p<0.05, **p<0.01, ***p<0.001 (Mann-Whitney test). 'ns' indicates non-significant differences. Abbreviations: FCM, flow cytometry; IFN, interferon; MDSC, myeloid-derived suppressor cell.

CCL7 drives the immunosuppressive properties of TAMs in CRC models

Recognizing that TAMs in CRC express high levels of CCL7, we examined whether tumor-derived cues regulate its production. Both M1 and M2a macrophages showed upregulation of CCL7, with M2a macrophages displaying slightly greater expression **(Figure 3a)**. Additionally, macrophages derived from CRC tumors (M2 phenotype) exhibited elevated CCL7 transcript levels **(Figure 3b)**. In vitro co-culture of BMDMs with MC38 cells resulted in a substantial increase in Ccl7 expression within macrophages. Similarly, exposure of naïve CD14+ monocytes to conditioned medium from HT29 cells led to an enrichment of CCL7+ macrophages and higher CCL7 secretion in the medium **(Figures 3c and 3d)**, indicating that tumor-secreted factors promote CCL7 production in myeloid cells.

Functionally, administering recombinant Ccl7 accelerated MC38 and CT26 tumor progression in vivo **(Figure 3e)**. Notably, this tumor-promoting effect was completely negated when macrophages were depleted in MC38-bearing mice **(Figure 3f)**.

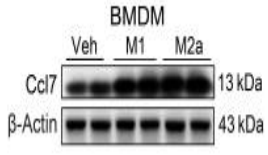

a)

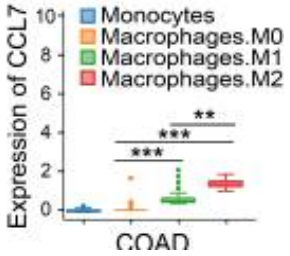

b)

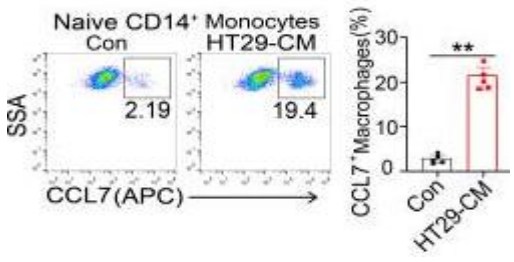

c)

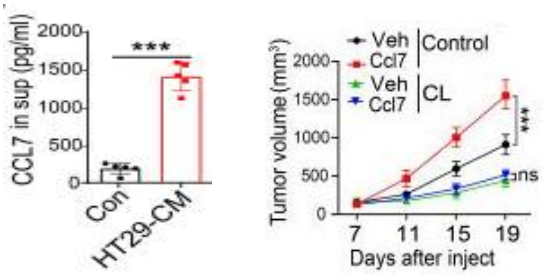

d) f)

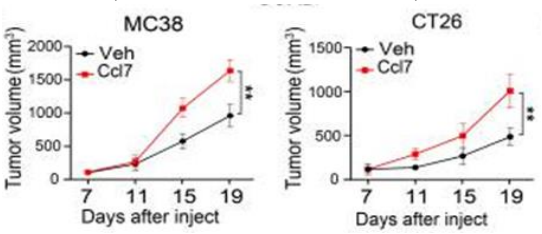

e)

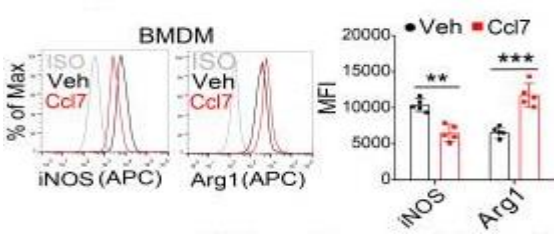

g)

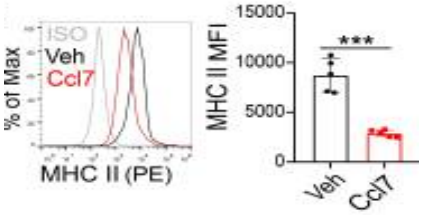

h)

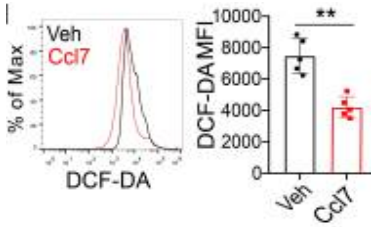

i)

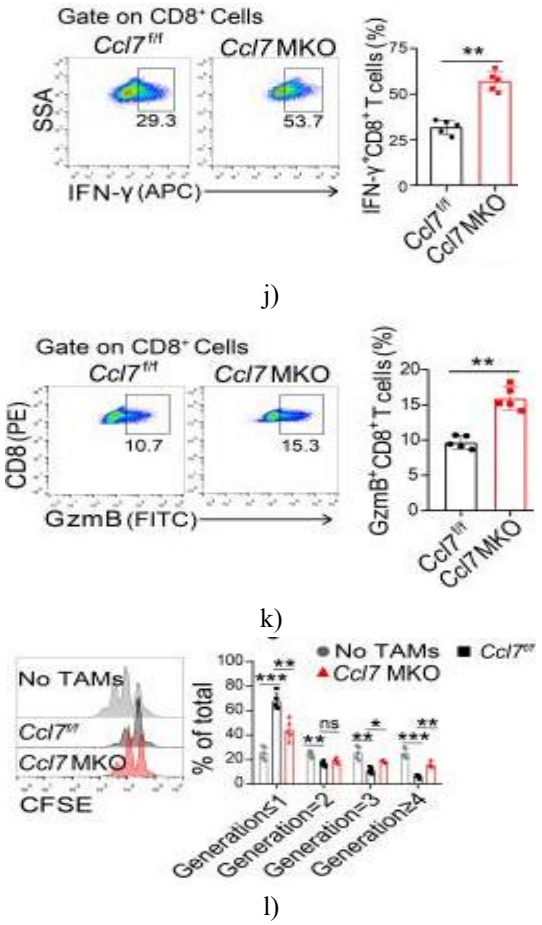

Figure 3. CCL7 enhances the immunosuppressive properties of TAMs. (a) BMDMs were polarized to M1 with 20 ng/mL LPS or to M2a with 20 ng/mL IL-4 for 24 hours, and CCL7 expression was analyzed by Western blot. (b) Expression of CCL7 in monocytes, M0, M1, and M2 macrophages from COAD tumor tissues was retrieved from the GEPIA2021 database. (c, d) Naïve CD14+ monocytes from healthy donors were exposed to 10% HT-29-conditioned medium for 24 hours; the proportion of CCL7+ macrophages was evaluated by FCM (c), and CCL7 concentration in the macrophage supernatant was measured (d, n=5). (e) Mice (6 weeks old) were subcutaneously injected with MC38 or CT26 cells and treated every three days with PBS (vehicle) or recombinant Ccl7 starting on day 3 post-injection; tumor growth was recorded (n=5). (f) MC38-bearing mice received recombinant Ccl7 treatment with or without clodronate liposomes (CL) to deplete macrophages, and tumor volumes were monitored (n=5). (g–i) BMDMs were treated with 1 µg/mL recombinant CCL7 for 48 hours; iNOS and Arg1 (g), MHC II (H), and ROS levels (DCF-DA) (i) were quantified via FCM (n=5). (j–l) CD8+ T cells were co-cultured with TAMs from Ccl7f/f or Ccl7 MKO mice at a 2:1 ratio; IFN-γ+ (j) and GzmB+ (k) T cell populations, as well as CD8+ T cell proliferation following anti-CD3/anti-CD28 stimulation (l), were assessed (n=5). Data are shown as mean ± SD; statistical analysis by Mann-Whitney test: *p<0.05, **p<0.01, ***p<0.001; ns = not significant. Abbreviations: FCM, flow cytometry; HD, healthy donor; IFN, interferon; TAMs, tumor-associated macrophages.

We next evaluated whether CCL7 modulates the immunosuppressive activity of TAMs. Exposure of BMDMs to recombinant Ccl7 increased Arg1 expression while simultaneously suppressing iNOS and MHC II levels **(Figures 3g and 3h)**. Consistently, Ccl7 treatment upregulated Arg1 and Mrc1 transcripts, while Nos2 and Tnfa expression was reduced. ROS production in CCL7-treated macrophages was also decreased **(Figure 3i)**. To further test the effect of CCL7 on TAM immunosuppressive function, CD8+ T cells were co-cultured with CCL7-deficient TAMs. In comparison with controls, the absence of CCL7 led to a higher proportion of IFN-γ+ and GzmB+ CD8+ T cells **(Figures 3j and 3k)**, and their proliferation was less suppressed **(Figure 3l)**, indicating that loss of CCL7 diminishes TAM-mediated immunosuppression. Collectively, these results indicate that tumor-derived factors drive the accumulation of CCL7-expressing TAMs, which in turn enhance immunosuppressive activity within the TIME.

CCL7-dependent lipid metabolism supports TAM immunosuppressive function

Lipid metabolic reprogramming is essential for TAMs to maintain their immunosuppressive phenotype. Therefore, we investigated whether CCL7 influences lipid metabolism in these cells. Gene set enrichment analysis (GSEA) revealed that CCL7+ TAMs are enriched for fatty acid metabolism and PPAR signaling pathways **(Figure 4a)**. Single-cell RNA-seq further identified upregulation of key lipid metabolic genes, including ACADVL, HADH, and PPARG, in CCL7+ TAMs **(Figure 4b)**. Both FCM and immunofluorescence assays demonstrated reduced fatty acid accumulation in CCL7-negative TAMs **(Figures 4c and 4d)**, while treatment with recombinant Ccl7 increased intracellular lipid droplet formation **(Figure 4e)**. Lipidomic profiling

confirmed that deletion of CCL7 reduced free fatty acid (FFA) levels in TAMs, whereas recombinant Ccl7 restored FFA content in BMDMs **(Figure 4f)**.

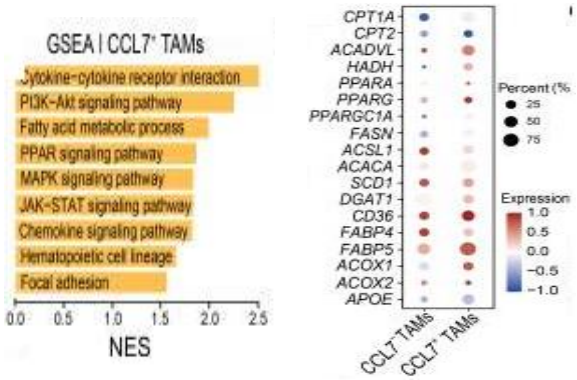

a) b)

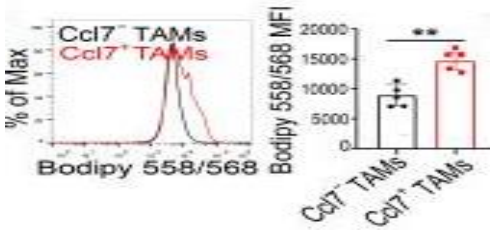

c)

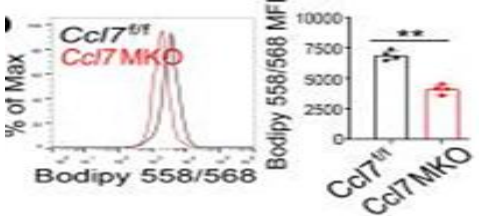

d)

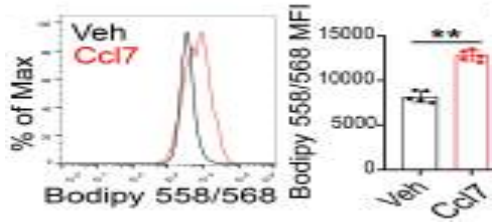

e)

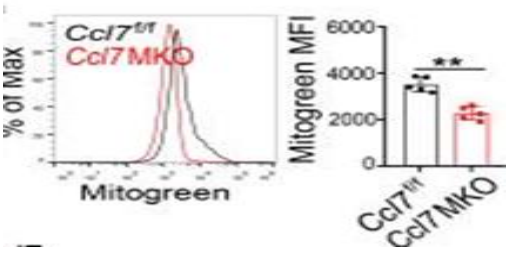

g)

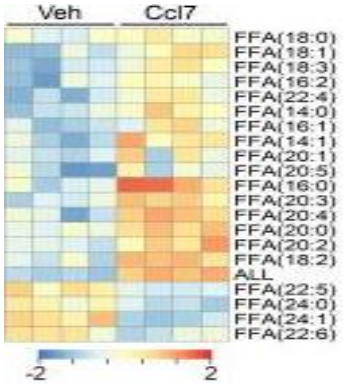

f)

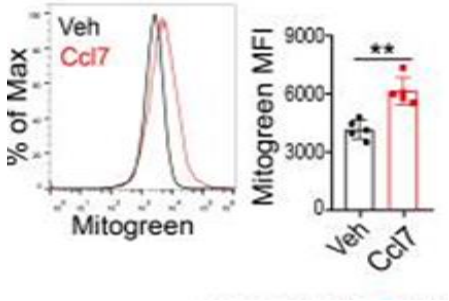

h)

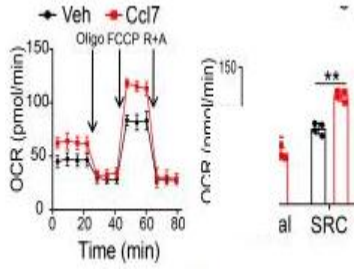

i)

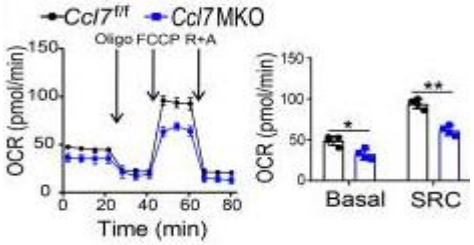

j)

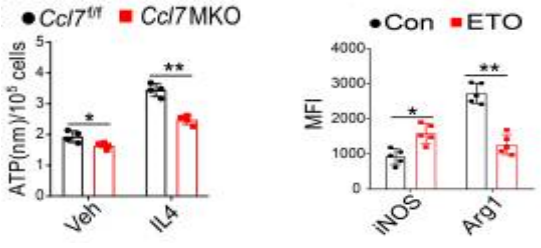

k) l)

Figure 4. CCL7 regulates fatty acid metabolism in TAMs. (a) GSEA was performed on genes ranked by

fold change between CCL7+ and CCL7– TAM clusters, with the normalized enrichment score (NES) reported. (b) A dot plot shows representative genes associated with fatty acid metabolism in both CCL7+ and CCL7– TAM populations. (c) Bodipy staining of CCL7+ and CCL7– TAMs from MC38 tumors. (d) Bodipy staining of BMDMs from Ccl7f/f and Ccl7 MKO mice analyzed by FCM; scale bar = 50 µm. (e) BMDMs treated with 1 µg/mL recombinant Ccl7 for 48 hours were stained with Bodipy (n=5). (f) Fatty acid intermediates in BMDMs treated with Ccl7 for 48 hours were quantified by LC-MS (n=4). (g) Mitochondrial content of TAMs from Ccl7f/f and Ccl7 MKO mice assessed using mitogreen staining (n=5). (h) Mitogreen staining of BMDMs after 48-hour Ccl7 exposure (n=5). (i, j) OCR and SRC were measured in BMDMs treated with recombinant Ccl7 (i) or derived from Ccl7f/f and Ccl7 MKO mice (j) using Seahorse XFe96 analyzer (n=4). (k) ATP production in BMDMs from Ccl7f/f and Ccl7 MKO mice treated ± IL-4 for 24 hours (n=4). (l) BMDMs treated with vehicle (0.1% DMSO) or etomoxir (ETO, 200 µM) for 24 hours were analyzed for iNOS and Arg1 by FCM (n=5). Data are mean ± SD; Mann-Whitney test: *p<0.05, **p<0.01, ***p<0.001. Abbreviations: BMDM= bone marrow-derived macrophages; ETO= etomoxir; GSEA= gene set enrichment analysis; OCR= oxygen consumption rate; SRC= spare respiratory capacity; TAMs= tumor-associated macrophages; DMSO= dimethylsulfoxide.

Given the central role of mitochondria in lipid metabolism [20], we investigated the effect of CCL7 on mitochondrial abundance in macrophages. FCM revealed that TAMs lacking CCL7 contained fewer mitochondria than controls, whereas Ccl7-treated macrophages showed increased mitochondrial numbers **(Figures 4g and 4h)**. Similarly, Ccl7 enhanced mitochondrial OCR and SRC, whereas CCL7-deficient macrophages had reduced OCR and SRC, indicating impaired FAO **(Figures 4i and 4j)**. ATP production was also diminished in CCL7-deficient macrophages **(Figure 4k)**. Additionally, treatment with the CPT1 inhibitor etomoxir suppressed Arg1 and elevated iNOS levels in BMDMs **(Figure 4l)**, suggesting that lipid metabolism is essential for TAM immunosuppressive function. These results collectively indicate that CCL7 enhances TAM immunosuppressive activity via upregulation of lipid metabolism.

CCL7 drives peroxisome biogenesis and FAO via PEX3

To explore how CCL7 modulates fatty acid metabolism, we conducted proteomic profiling. This analysis identified 523 upregulated and 409 downregulated proteins in Ccl7f/f TAMs **(Figure 5a)**. Notably, proteins associated with peroxisomes and lysosomes were enriched in Ccl7f/f TAMs **(Figure 5b)**. Considering the role of peroxisomes in lipid metabolism and ROS detoxification [21], we hypothesized that CCL7 promotes FAO and ROS clearance through peroxisomal function. Both proteomic and qPCR data highlighted differential expression of peroxisome-related genes, with Pex3 showing the strongest change **(Figures 5c and 5d)**. Western blot confirmed reduced Pex3 expression in Ccl7 MKO TAMs, while Ccl7 treatment increased Pex3 levels **(Figure 5e).**

PMP70, a peroxisomal marker, decreased in Ccl7 MKO TAMs and increased after Ccl7 treatment **(Figures 5f and 5g)**. Overexpressing Pex3 in Ccl7 MKO TAMs restored PMP70, FAO, and ROS clearance, increased Arg1, and decreased iNOS expression, indicating Pex3's role in FAO and ROS regulation. Conversely, Pex3 knockdown via siRNA reduced FAO and increased ROS **(Figures 5h and 5i)**, increased iNOS, and decreased Arg1 **(Figure 5j)**. Functionally, siPex3 macrophages enhanced anti-CD3/anti-CD28-induced CD8+ T cell proliferation and IFN-γ production **(Figures 5k and 5l)**. These data strongly suggest that CCL7 promotes peroxisome biogenesis and FAO in TAMs, reinforcing their immunosuppressive function through PEX3.

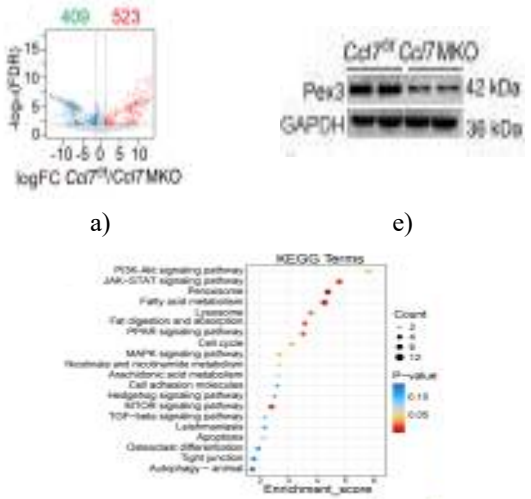

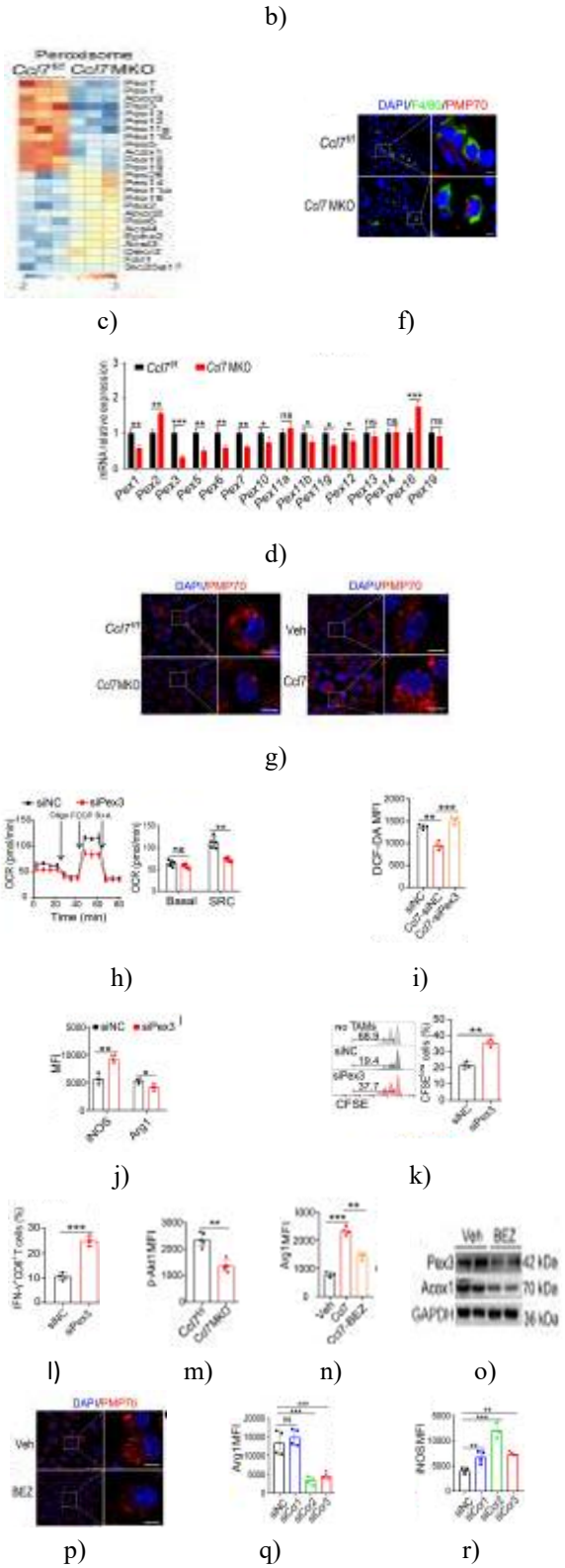

Figure 5. CCL7 promotes PEX3-mediated fatty acid metabolism in TAMs. (a–c) Differentially expressed proteins in Ccl7f/f and Ccl7 MKO TAMs from MC38 tumors were visualized via volcano plot (a), KEGG pathway enrichment (b), and a heatmap of peroxisome-related proteins (c) (n=3). (d) Peroxisome-associated gene expression in TAMs from Ccl7f/f and Ccl7 MKO tumor tissues (n=3). (e) Western blot analysis of Pex3 in BMDMs from Ccl7f/f and Ccl7 MKO mice. (f) Representative PMP70 immunostaining (red) in TAMs from Ccl7f/f and Ccl7 MKO tumors; scale bar = 5 μm. (g) PMP70 expression in BMDMs from Ccl7f/f, Ccl7 MKO, and recombinant Ccl7-treated BMDMs (24 h). (h) OCR and SRC measurements in BMDMs transfected with siPex3 (n=5). (i) ROS levels in siPex3-transfected BMDMs following 24 h Ccl7 stimulation (n=4). (j) iNOS and Arg1 levels in siPex3 BMDMs assessed by FCM (n=4). (K, L) CD8+ T cells co-cultured with siNC or siPex3 TAMs at a 2:1 ratio; proliferation (k) and IFN-γ production (l) were measured (n=4). (m) Intracellular p-Akt1 staining in TAMs from Ccl7f/f or Ccl7 MKO tumor-bearing mice (n=5). (n) BMDMs pretreated ± BEZ235 (200 nM) and then stimulated with Ccl7 for 24 h; Arg1 levels measured (n=4). (o–p) Western blot analysis of Pex3 and Acox1 (o) and PMP70 expression (p) in BMDMs ± BEZ235. (q, r) Arg1 (q) and iNOS (r) expression in BMDMs transfected with siRNAs targeting Ccr1, Ccr2, and Ccr3. Data are mean ± SD; Mann-Whitney test: *p<0.05, **p<0.01, ***p<0.001; ns = not significant. Abbreviations: BMDM= bone marrow-derived macrophages; FCM= flow cytometry; IFN= interferon; TAMs= tumor-associated macrophages; KEGG= Kyoto Encyclopedia of Genes and Genomes; GAPDH= glyceraldehyde-3-phosphate dehydrogenase.

To explore how CCL7 enhances PEX3 in TAMs, RNA-seq analysis of tumor-infiltrating TAMs was performed. Compared to Ccl7 MKO TAMs, Ccl7f/f TAMs showed 903 upregulated and 498 downregulated genes, enriched in cytokine-cytokine receptor interaction, PI3K-Akt signaling, and cell cycle pathways. Among these, PI3K-Akt signaling exhibited the strongest enrichment; 33 differentially expressed genes, including Itga3, Irs1, and Ccnd1, were identified in CCL7-deficient TAMs. FCM confirmed reduced p-Akt levels in CCL7-deficient TAMs **(Figure 5m)**. Validation via qPCR of 10 selected PI3K-Akt pathway genes mirrored RNA-seq results, while western blot revealed diminished p-PI3K and p-Akt proteins upon CCL7 deletion. Recombinant CCL7

restored p-PI3K and p-AKT levels in BMDMs. Treatment with the PI3K inhibitor BEZ235 significantly blocked CCL7-induced upregulation of Arg1 and Mrc1 **(Figure 5n)** and reduced Pex3 and Acox1 expression **(Figure 5o)**, also lowering PMP70 levels, indicative of fewer peroxisomes **(Figure 5p)**. These data suggest that CCL7 promotes PEX3 expression in TAMs via PI3K-AKT signaling.

Analysis of CCL7 receptor expression revealed that CCR1 was broadly present across multiple cell types, CCR3 primarily in CD4+ T cells, and CCR2 restricted to myeloid cells, particularly macrophages and monocytes, within the CRC TIME. All three receptors were upregulated in TAMs compared to splenic macrophages. To determine receptor involvement in CCL7-mediated immunosuppression and PEX3 regulation, BMDMs were transfected with siRNAs targeting Ccr1, Ccr2, and Ccr3. Knockdown of Ccr2 or Ccr3 reduced Arg1 expression in CCL7-treated BMDMs **(Figure 5q)** and increased M1 markers including iNOS, TNFα, and IL-1β **(Figure 5r)**. Considering CCR3 is mainly expressed in CD4+ T cells and CCR2 predominantly in macrophages, CCR2 was selected for further study. Knockdown of Ccr2 decreased p-PI3K, p-Akt1, and Pex3 levels in BMDMs and inhibited TAM immunosuppressive activity. Collectively, these findings demonstrate that CCL7 promotes PEX3 expression and enhances TAM immunosuppressive function through the PI3K-AKT-CCR2 signaling axis.

CCL7-CCR2 signaling suppresses CD8+ T cell infiltration via AKT2-STAT1-CXCL10 inhibition in the tumor microenvironment

Beyond its established role in promoting tumor cell migration [13], we investigated how CCL7 influences the trafficking of immune cells within the colorectal tumor microenvironment. TAMs from Ccl7 MKO mice showed a pronounced reduction in the expression of chemokines, including Ccl7, Ccl6, Ccl17, and Ccl12, compared with TAMs from Ccl7f/f controls **(Figures 6a and 6b)**. ELISA analysis of the TAM-conditioned media confirmed these decreases in chemokine secretion upon Ccl7 deletion. Notably, the absence of Ccl7 was associated with a marked upregulation of Cxcl10 **(Figure 6a)**, a chemokine critical for directing cytotoxic CD8+ T cells to tumor sites [22].

We hypothesized that this increased CXCL10 expression in Ccl7-deficient TAMs could account for the enhanced CD8+ T cell recruitment observed. Indeed, serum CXCL10 levels were significantly higher in MC38 tumor-bearing Ccl7 MKO mice than in their Ccl7f/f counterparts **(Figure 6c)**, whereas other T cell–recruiting chemokines, such as Ccl5 and Cxcl9, remained unchanged.

Functionally, CD8+ T cells displayed stronger migration toward conditioned media from Ccl7 MKO TAMs than toward control media **(Figure 6d)**. Consistently, in vivo adoptive transfer experiments confirmed that CD8+ T cell infiltration into MC38 tumors was significantly increased when TAMs lacked Ccl7 **(Figure 6e)**. These results indicate that the loss of Ccl7 in TAMs promotes T cell infiltration, likely through the elevated production of CXCL10, revealing a key mechanism by which CCL7-CCR2 signaling restrains antitumor immunity within the TIME.

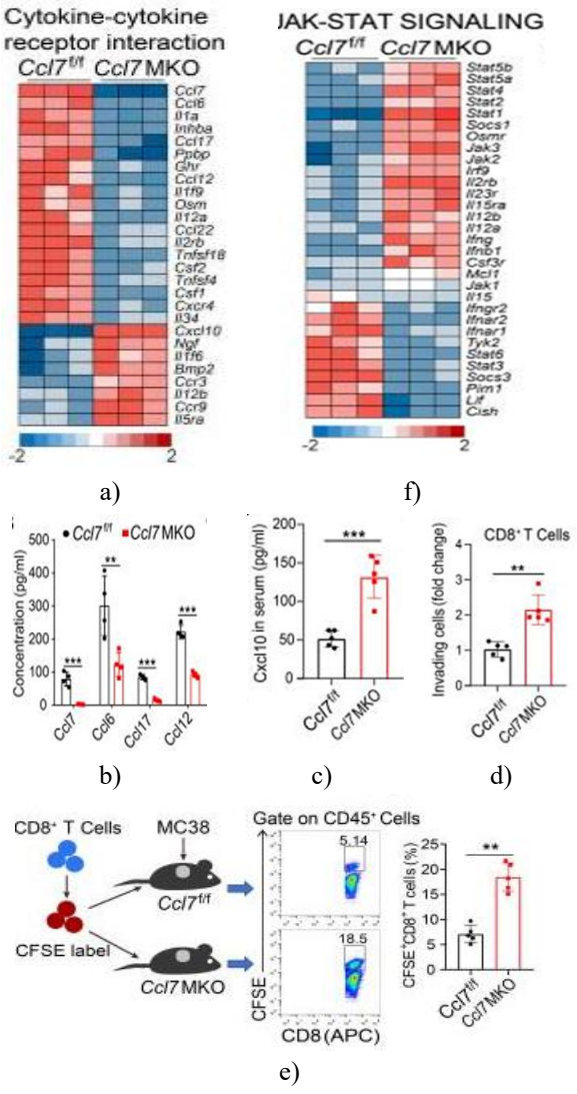

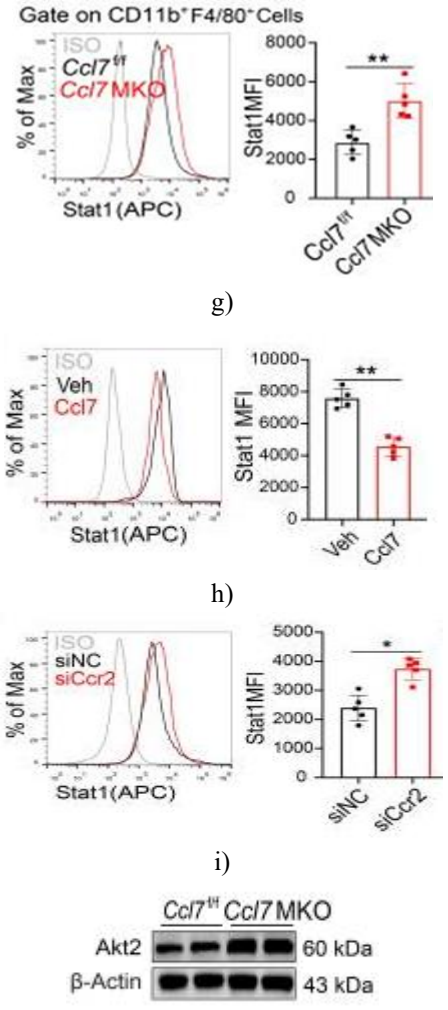

Figure 6. CCL7 restricts CD8+ T-cell infiltration by suppressing the AKT2-STAT1-CXCL10 axis. (a) Cytokine-cytokine receptor interaction genes showing differential expression in TAMs from Ccl7f/f versus Ccl7 MKO tumors. (b) Concentrations of Ccl7, Ccl6, Ccl17, and Ccl12 in TAM-conditioned media from Ccl7f/f and Ccl7 MKO mice. (c) Serum levels of Cxcl10 in MC38 tumor-bearing Ccl7f/f and Ccl7 MKO mice. (d) Migration assay quantifying CD8+ T-cell movement toward conditioned medium from TAMs of Ccl7f/f and Ccl7 MKO mice (n=5). (e) In vivo tracking of CFSE-labeled CD8+ T cells transferred into MC38 tumor-bearing mice; tumor infiltration was measured 18 hours later (n=5). (f) Genes in the JAK-STAT pathway differentially expressed in TAMs from Ccl7f/f and Ccl7 MKO tumors. (g) Stat1 protein levels in TAMs of Ccl7f/f versus Ccl7 MKO tumors. (h) Stat1 levels in BMDMs after recombinant Ccl7 stimulation, analyzed by FCM. (i) Akt2 expression in TAMs from Ccl7f/f and Ccl7 MKO mice. (j) Stat1 expression in BMDMs after Ccr2 knockdown. Data are mean±SD; statistical significance by Mann-Whitney test (*p<0.05, **p<0.01, ***p<0.001). BMDM= bone marrow-derived macrophages; FCM= flow cytometry; TAMs= tumor-associated macrophages.

It is established that IFN-γ triggers CXCL10 production via JAK/STAT1 signaling [23]. Consistent with this, TAMs from Ccl7 MKO tumors exhibited elevated Stat1 compared to Ccl7f/f TAMs **(Figures 6f and 6g)**. Treatment with recombinant Ccl7 lowered Stat1 expression in BMDMs, whereas Stat1 increased upon Ccr2 knockdown **(Figures 6h and 6i)**. Prior reports indicate AKT2 is elevated in M1 macrophages and regulates STAT1/NF-κB pathways [24, 25]. Here, Akt2 levels rose in TAMs lacking Ccl7 and further increased when Ccr2 was silenced **(Figure 6j)**. These observations indicate that CCL7 interacts with CCR2 to dampen the AKT2-STAT1-CXCL10 pathway, thereby limiting CD8+ T-cell infiltration into tumors.

Blocking CCL7 inhibits CRC progression and enhances anti-PD-L1 immune responses

We tested whether targeting CCL7 could impede tumor growth. Administration of Ccl7-neutralizing antibodies or the inhibitor bindarit effectively slowed growth of MC38 and CT26 tumors and improved survival of tumor-bearing mice **(Figures 7a and 7b)**. Both treatments reduced TAM density within tumors **(Figure 7c)**. FCM revealed that inhibition of CCL7 increased M1-like TAMs and decreased M2-like TAMs in MC38 tumors **(Figures 7d and 7d)**. Bindarit treatment notably decreased intratumoral Ccl7+ TAMs and reduced serum Ccl7. TAMs from treated tumors displayed higher Stat1 expression **(Figure 7f)**, and CD8+ T cells showed increased IFN-γ and TNFα production **(Figure 7g)**. Together, these results indicate that CCL7 blockade not only suppresses tumor growth but also reprograms the tumor immune microenvironment.

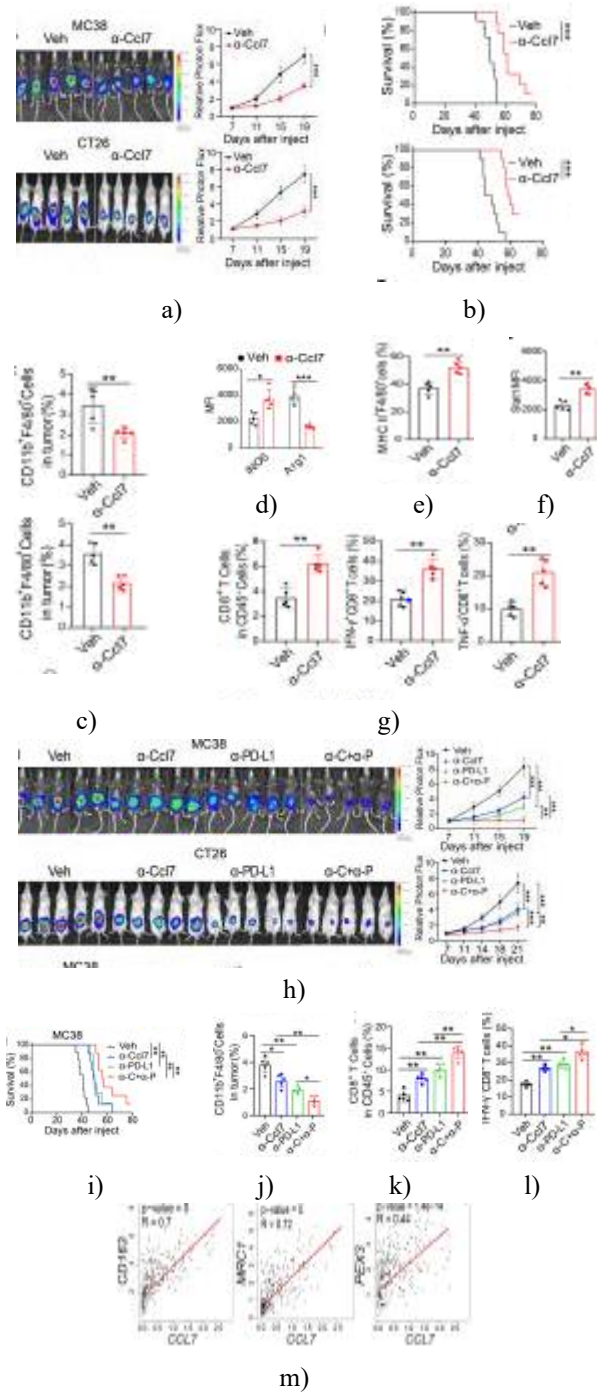

Figure 7. Targeting CCL7 potentiates anti-PD-L1 immunotherapy. (a–g) MC38-luc and CT26-luc tumor cells were injected intraperitoneally into mice, which then received either 100 μg of anti-Ccl7 antibody (α-Ccl7) or vehicle (PBS) every 3 days, starting from day 7 after tumor implantation. Tumor progression was tracked (a), and survival of tumor-bearing mice was analyzed (b, n=9–12). TAM percentages were determined (c), along with macrophage polarization markers iNOS and Arg1 (d), the frequency of MHC II+ TAMs (e), Stat1 levels in TAMs (f), and the proportion of IFN-γ+ and TNF-α+ CD8+ T cells (g), with n=5. (h–l) C57 and BALB/c mice injected with MC38-luc or CT26-luc cells were treated with vehicle, α-Ccl7, anti-PD-L1 (αPD-L1), or their combination (α-C+α-P). Tumor growth (h), survival (I, n=10–14), and tumor-infiltrating immune populations, including TAMs (j), CD8+ T cells (k), and IFN-γ+ CD8+ T cells (l), were assessed by FCM (n=5). (m) Correlations of CCL7 expression with CD163, MRC1, and PEX3 in human CRC tissues. Data are mean±SD. Statistical analyses were performed using Mann-Whitney (a, c–g), log-rank test (b, i), and one-/two-way ANOVA with Sidak correction (h, j–l), with *p<0.05, **p<0.01, ***p<0.001. CRC= colorectal cancer; IFN= interferon; TAMs= tumor-associated macrophages.

Considering that CCL7 blockade significantly increases tumor-infiltrating IFN-γ+ CD8+ T cells, and that IFN-γ signaling enhances PD-L1 expression in TAMs [26], we tested whether neutralizing CCL7 could boost anti-PD-L1 therapy. Co-administration of anti-CCL7 and anti-PD-L1 antibodies led to stronger suppression of tumor growth and improved survival of tumor-bearing mice **(Figures 7h and 7i)**. TAM density within tumors decreased further, while CD8+ T-cell activation was augmented **(Figures 7j–7l)**. Bioinformatics analyses showed positive correlations between CCL7 and CD163, MRC1, and PEX3 in CRC patient samples **(Figure 7m)**. Collectively, these data reinforce the role of CCL7 in modulating tumor-infiltrating CD8+ T cells and macrophages, influencing tumor progression and resistance to immune checkpoint inhibitors.

Immune checkpoint blockade has emerged as a transformative strategy in oncology, yet a subset of CRC patients, including those with MSI-H/dMMR, exhibit poor responses to anti-PD-1/PD-L1 therapies. Understanding how the tumor immune microenvironment (TIME) contributes to this non-responsiveness is critical, as the intensity and composition of immune infiltration largely determine therapeutic efficacy [27]. In this study, we demonstrate that CCL7+ TAMs facilitate resistance to ICIs in CRC, identifying CCL7 as a potential target for overcoming PD-1/PD-L1 therapy refractoriness.

CCL7 is a chemokine traditionally recognized for recruiting monocytes, dendritic cells, and activated T

lymphocytes to inflammatory sites [19]. However, emerging evidence indicates that CCL7 expression can support tumor development in breast cancer, renal cell carcinoma, and CRC [19]. Our findings show that CCL7 deletion impairs both the chemotactic and immunosuppressive properties of TAMs, indicating that in the CRC TIME, CCL7 does not act as a conventional proinflammatory mediator. While previous studies have suggested both tumor-promoting and tumor-suppressive roles for CCL7 [28], our results indicate that in CRC, CCL7 enhances TAM-mediated immunosuppression. Monocyte-derived MDSC-secreted CCL7 can engage CCR2 on tumor cells to activate the JNK/STAT3 pathway, driving proliferation of dormant CRC cells [17], and can also signal through CCR3 to promote proliferation, invasion, and migration via ERK and JNK pathways [15]. In our study, CCR2 and CCR3 mediate CCL7-induced immunosuppressive activity in macrophages, with CCR2 appearing to play a dominant role. Moreover, CCL7 facilitates peroxisome biogenesis and fatty acid oxidation in TAMs, augmenting their immunosuppressive function and contributing to the establishment of an inhibitory TIME in CRC.

Peroxisomes are specialized membrane-bound organelles responsible for key metabolic processes, including fatty acid oxidation (FAO) and reactive oxygen species (ROS) metabolism [21]. In mammalian cells, peroxisome formation is orchestrated by peroxins, a diverse set of proteins such as PEX3, PEX16, and PEX19, which are essential for peroxisome regeneration [21]. Our data revealed that several peroxins, especially PEX3, are highly expressed in CCL7+ TAMs, indicating that PEX3 is a pivotal regulator of FAO and ROS handling in these cells. Previous studies have shown that PEX3 can modulate phospholipid metabolism and activate the AKT/GSK3β signaling pathway through ITGB3 localization at the plasma membrane [29]. In the present study, we found that CCL7 upregulates PEX3 in TAMs, thereby reinforcing their immunosuppressive activity via the CCR2-PI3K-AKT pathway. This suggests a potential feedback loop between PEX3 and PI3K-AKT signaling that sustains FAO and enhances TAM-mediated immunosuppression [30]. The PI3K/Akt pathway, triggered by multiple receptor-mediated signals, is critical for balancing pro- and anti-inflammatory macrophage functions [31]. Notably, AKT isoforms exhibit distinct roles: AKT1 promotes M2 polarization and immunosuppressive functions, whereas AKT2 favors M1 polarization and anti-tumor activity [32]. Our results indicate that CCL7-CCR2 signaling inhibits AKT2 while activating AKT1, highlighting its regulatory role in macrophage polarization, although the underlying molecular mechanisms warrant further investigation.

We demonstrated that blocking CCL7 reduces TAM infiltration and enhances CD8+ T-cell recruitment. CCL7-deficient TAMs promote CD8+ T-cell migration through the AKT2-STAT1-CXCL10 axis. IFN-γ secreted by these T cells may, in turn, upregulate immune checkpoints such as PD-L1, potentially contributing to tumor immune escape [33]. Moreover, combining anti-CCL7 with anti-PD-L1 therapy synergistically suppresses CRC growth in murine models. These findings suggest that CCL7 mediates resistance to ICI therapy by regulating the abundance and activity of TAMs and tumor-infiltrating CD8+ T cells, making it a promising target for combination immunotherapy.

Previous research has shown that Bindarit reduces tumor growth and TAM infiltration in human melanoma cells, inducing tumor cell necrosis [34]. Similarly, Bindarit treatment in mouse models of breast and prostate cancer significantly inhibited tumor progression and decreased TAM accumulation [35]. In models of autoimmune disease, Bindarit protected lupus-prone mice from kidney injury and prolonged survival [36]. Additionally, in animal models of arterial injury, Bindarit reduced neointima formation by acting on vascular smooth muscle cells and decreasing macrophage content [37]. These findings collectively suggest that Bindarit or anti-CCL7 antibodies could be applied broadly in cancer therapy and autoimmune disease management. Further studies are needed to explore the therapeutic potential of CCL7 inhibition in oncology and autoimmunity.

Our study primarily highlights that elevated CCL7+ TAM levels in CRC tissues correlate with patient resistance to ICI therapy. However, the clinical data are preliminary, and the utility of CCL7 as a biomarker for ICI resistance requires validation in larger patient cohorts, particularly those with documented immunotherapy outcomes. Moreover, the development of orthotopic tumor models could more accurately recapitulate the tumor microenvironment (TME) of primary CRC, providing a robust platform for investigating CCL7-CCR2 signaling within the TIME prior to clinical translation.

Conclusion

In conclusion, CCL7+ TAMs are enriched in CRC patients exhibiting tolerance to ICI therapy. TAM-derived CCL7 regulates the accumulation and function of tumor-infiltrating CD8+ T cells and macrophages, influencing tumor progression. Blocking CCL7 enhances the anti-tumor efficacy of PD-L1 blockade, highlighting its role in sustaining TAM immunosuppression while inhibiting CD8+ T-cell chemotaxis. These findings underscore CCL7 as a potential therapeutic target for combination ICI-based immunotherapy in CRC.

Acknowledgments: The authors appreciate members of our laboratories for their kind suggestions.

Conflict of Interest: None

Financial Support: This work was supported by the National Natural Science Foundation of China (nos. 82271885, 82572105, and 32470971), the major project of joint medical research of science and health in Chongqing (2025DBXM006), the Middle-Aged and Young Medical Talent Project of Chongqing, the National Outstanding Youth Reserve Talent Training Project (no. HBRC202406), the Natural Science Foundation of Chongqing (no. 2024NSCQKJFZMSX0059), the Chongqing Natural Science Foundation Innovation and Development Joint Fund Project (no. CSTB2025NSCQ-LZX0004), and the Funding for Chongqing Young and Middle-Aged Medical Excellence Team.

Ethics Statement: All experiments were conducted in compliance with local, national, and international regulations and were approved by the Ethics Committee of the hospital under protocol CZLS2023114-A.

References

1. Li Q, Geng S, Luo H, et al. Signaling pathways involved in colorectal cancer: pathogenesis and targeted therapy. Signal Transduct Target Ther. 2024;9:266. doi: 10.1038/s41392-024-01953-7
2. Thomas EM, Wright JA, Blake SJ, et al. Advancing translational research for colorectal immuno-oncology. Br J Cancer. 2023;129:1442–50. doi: 10.1038/s41416-023-02392-x
3. Meyiah A, Khan FI, Alfaki DA, et al. The colorectal cancer microenvironment: Preclinical progress in identifying targets for cancer therapy. Transl Oncol. 2025;53:102307. doi: 10.1016/j.tranon.2025.102307
4. Chu X, Li X, Zhang Y, et al. Integrative single-cell analysis of human colorectal cancer reveals patient stratification with distinct immune evasion mechanisms. Nat Cancer . 2024;5:1409–26. doi: 10.1038/s43018-024-00807-z
5. Chen Y, Wang D, Li Y, et al. Spatiotemporal single-cell analysis decodes cellular dynamics underlying different responses to immunotherapy in colorectal cancer. Cancer Cell. 2024;42:1268–85. doi: 10.1016/j.ccell.2024.06.009
6. Rooney MS, Shukla SA, Wu CJ, et al. Molecular and genetic properties of tumors associated with local immune cytolytic activity. Cell. 2015;160:48–61. doi: 10.1016/j.cell.2014.12.033
7. Park S-Y, Pylaeva E, Bhuria V, et al. Harnessing myeloid cells in cancer. Mol Cancer. 2025;24:69. doi: 10.1186/s12943-025-02249-2
8. Wu L, Zhang X, Zheng L, et al. RIPK3 Orchestrates Fatty Acid Metabolism in Tumor-Associated Macrophages and Hepatocarcinogenesis. Cancer Immunol Res. 2020;8:710–21. doi: 10.1158/2326-6066.CIR-19-0261
9. Van Damme J, Proost P, Lenaerts JP, et al. Structural and functional identification of two human, tumor-derived monocyte chemotactic proteins (MCP-2 and MCP-3) belonging to the chemokine family. J Exp Med. 1992;176:59–65. doi: 10.1084/jem.176.1.59
10. Chang TT, Chen C, Chen JW. CCL7 as a novel inflammatory mediator in cardiovascular disease, diabetes mellitus, and kidney disease. Cardiovasc Diabetol. 2022;21:185. doi: 10.1186/s12933-022-01626-1
11. Jung D-W, Che ZM, Kim J, et al. Tumor-stromal crosstalk in invasion of oral squamous cell carcinoma: a pivotal role of CCL7. Int J Cancer. 2010;127:332–44. doi: 10.1002/ijc.25060
12. Hwang T-L, Lee L-Y, Wang C-C, et al. CCL7 and CCL21 overexpression in gastric cancer is associated with lymph node metastasis and poor prognosis. World J Gastroenterol. 2012;18:1249–56. doi: 10.3748/wjg.v18.i11.1249
13. Han S, Wang T, Chen Y, et al. High CCL7 expression is associated with migration, invasion and bone metastasis of non-small cell lung cancer cells. Am J Transl Res. 2019;11:442–52
14. Yang H, Jian L, Jin Q, et al. CCL7 playing a dominant role in recruiting early OCPs to facilitate

osteolysis at metastatic site of colorectal cancer. Cell Commun Signal. 2022;20:94. doi: 10.1186/s12964-022-00867-7

15. Lee YS, Kim S-Y, Song SJ, et al. Crosstalk between CCL7 and CCR3 promotes metastasis of colon cancer cells via ERK-JNK signaling pathways. Oncotarget. 2016;7:36842–53. doi: 10.18632/oncotarget.9209
16. Xu Z, Gao H, Zhang Y, et al. CCL7 and TGF-β secreted by MSCs play opposite roles in regulating CRC metastasis in a KLF5/CXCL5-dependent manner. Mol Ther. 2022;30:2327–41. doi: 10.1016/j.ymthe.2022.03.005
17. Ren X, Xiao J, Zhang W, et al. Inhibition of CCL7 derived from Mo-MDSCs prevents metastatic progression from latency in colorectal cancer. Cell Death Dis. 2021;12:484. doi: 10.1038/s41419-021-03698-5]
18. Li J, Wu C, Hu H, et al. Remodeling of the immune and stromal cell compartment by PD-1 blockade in mismatch repair-deficient colorectal cancer. Cancer Cell. 2023;41:1152–69. doi: 10.1016/j.ccell.2023.04.011
19. Chidimatsu H, Tsunedomi R, Nakagami Y, et al. Serum CCL7 Is a Novel Prognostic Biomarker of Metastatic Colorectal Cancer. Anticancer Res. 2023;43:105–14. doi: 10.21873/anticanres.16139
20. Netea-Maier RT, Smit JWA, Netea MG. Metabolic changes in tumor cells and tumor-associated macrophages: A mutual relationship. Cancer Lett. 2018;413:102–9. doi: 10.1016/j.canlet.2017.10.037. [DOI] [PubMed] [Google Scholar]
21. Jo DS, Park NY, Cho DH. Peroxisome quality control and dysregulated lipid metabolism in neurodegenerative diseases. Exp Mol Med. 2020;52:1486–95. doi: 10.1038/s12276-020-00503-9
22. Kohli K, Pillarisetty VG, Kim TS. Key chemokines direct migration of immune cells in solid tumors. Cancer Gene Ther. 2022;29:10–21. doi: 10.1038/s41417-021-00303-x
23. Shi D, Li Y, Shi X, et al. Transcriptional expression of CXCL10 and STAT1 in lupus nephritis and the intervention effect of triptolide. Clin Rheumatol. 2023;42:539–48. doi: 10.1007/s10067-022-06400-y
24. Ghosh S, Stepicheva N, Yazdankhah M, et al. The role of lipocalin-2 in age-related macular degeneration (AMD) Cell Mol Life Sci. 2020;77:835–51. doi: 10.1007/s00018-019-03423-8
25. Clarke DL, Clifford RL, Jindarat S, et al. TNFα and IFNγ synergistically enhance transcriptional activation of CXCL10 in human airway smooth muscle cells via STAT-1, NF-κB, and the transcriptional coactivator CREB-binding protein. J Biol Chem. 2010;285:29101–10. doi: 10.1074/jbc.M109.0999952
26. Abiko K, Matsumura N, Hamanishi J, et al. IFN-γ from lymphocytes induces PD-L1 expression and promotes progression of ovarian cancer. Br J Cancer. 2015;112:1501–9. doi: 10.1038/bjc.2015.101
27. Solinas G, Schiarea S, Liguori M, et al. Tumor-conditioned macrophages secrete migration-stimulating factor: a new marker for M2-polarization, influencing tumor cell motility. J Immunol. 2010;185:642–52. doi: 10.4049/jimmunol.1000413
28. Wu Z, Bai X, Lu Z, et al. LINC01094/SPI1/CCL7 Axis Promotes Macrophage Accumulation in Lung Adenocarcinoma and Tumor Cell Dissemination. J Immunol Res. 2022;2022:6450721. doi: 10.1155/2022/6450721.
29. Sun J-T, Wang Z-M, Zhou L-H, et al. PEX3 promotes regenerative repair after myocardial injury in mice through facilitating plasma membrane localization of ITGB3. Commun Biol. 2024;7:795. doi: 10.1038/s42003-024-06483-0.
30. He Y, Sun MM, Zhang GG, et al. Targeting PI3K/Akt signal transduction for cancer therapy. Signal Transduct Target Ther. 2021;6:425. doi: 10.1038/s41392-021-00828-5
31. Linton MF, Moslehi JJ, Babaev VR. Akt Signaling in Macrophage Polarization, Survival, and Atherosclerosis. Int J Mol Sci. 2019;20:20.:2703. doi: 10.3390/ijms20112703
32. Vergadi E, Ieronymaki E, Lyroni K, et al. Akt Signaling Pathway in Macrophage Activation and M1/M2 Polarization. J Immunol. 2017;198:1006–14. doi: 10.4049/jimmunol.1601515
33. Moon JW, Kong S-K, Kim BS, et al. IFNγ induces PD-L1 overexpression by JAK2/STAT1/IRF-1 signaling in EBV-positive gastric carcinoma. Sci Rep. 2017;7:17810. doi: 10.1038/s41598-017-18132-0
34. Gazzaniga S, Bravo AI, Guglielmotti A, et al. Targeting tumor-associated macrophages and inhibition of MCP-1 reduce angiogenesis and tumor growth in a human melanoma xenograft. J Invest

Dermatol. 2007;127:2031–41. doi: 10.1038/sj.jid.5700827

35. Zollo M, Di Dato V, Spano D, et al. Targeting monocyte chemotactic protein-1 synthesis with bindarit induces tumor regression in prostate and breast cancer animal models. Clin Exp Metastasis. 2012;29:585–601. doi: 10.1007/s10585-012-9473-5
36. Zoja C, Corna D, Benedetti G, et al. Bindarit retards renal disease and prolongs survival in murine lupus autoimmune disease. Kidney Int. 1998;53:726–34. doi: 10.1046/j.1523-1755.1998.00804.x.
37. Grassia G, Maddaluno M, Guglielmotti A, et al. The anti-inflammatory agent bindarit inhibits neointima formation in both rats and hyperlipidaemic mice. Cardiovasc Res. 2009;84:485–93. doi: 10.1093/cvr/cvp238